Journal of Geophysical Research: Biogeosciences

RESEARCH ARTICLE
10.1029/2018JG004637

Partitioning Eddy Covariance Water Flux Components Using Physiological and Micrometeorological Approaches

Oscar Perez-Priego[1], Gabriel Katul[2], Markus Reichstein[1], Tarek S. El-Madany[1], Bernhard Ahrens[1], Arnaud Carrara[3], Todd M. Scanlon[4], and Mirco Migliavacca[1]

[1]Max Planck Institute for Biogeochemistry, Jena, Germany, [2]Nicholas School of the Environment and Earth Sciences, Duke University, Durham, NC, USA, [3]Fundación Centro de Estudios Ambientales del Mediterráneo (CEAM), Valencia, Spain, [4]Department of Environmental Sciences, University of Virginia, Charlottesville, VA, USA

Key Points:
- A novel approach for partitioning eddy covariance water fluxes into their constitutive components is proposed using optimality principles
- The approach was independently tested with lysimeter measurements, as well as benchmarked with other existing micrometeorological approaches
- This approach provides new perspectives on water partitioning, which can be utilized across a wide range of climate conditions and biomes

Supporting Information:
- Supporting Information S1

Correspondence to:
O. Perez-Priego,
opriego@mpg-jena.mpg;
oscarperezpriego@gmail.com

Citation:
Perez-Priego, O., Katul, G., Reichstein, M., El-Madany, T. S., Ahrens, B., Carrara, A., et al. (2018). Partitioning eddy covariance water flux components using physiological and micrometeorological approaches. *Journal of Geophysical Research: Biogeosciences*, *123*. https://doi.org/10.1029/2018JG004637

Received 4 JUN 2018
Accepted 24 AUG 2018
Accepted article online 29 AUG 2018

Abstract Eddy covariance (EC) provides ecosystem-scale estimates of photosynthesis (P_h) and evapotranspiration (ET; the sum of plant transpiration [T] and evaporation [E_s]). Separating ET into its components is becoming necessary for linking plant-water use strategies to environmental variability. Based on optimality principles, a data-model based approach for partitioning ET was proposed and independently tested. Short-term responses of canopy-scale *internal* leaf-to-ambient CO_2 (χ) were predicted based on a big-leaf representation of the canopy accounting for the influence of boundary-layer conductance. This representation allowed investigating stomatal behavior in accordance with the P_h estimates. With the objective of minimizing the carbon cost of transpiration, a novel optimization approach was implemented to develop solutions for an optimal stomatal conductance model as the basis to derive T. The E_s was then calculated as a residual between the observed ET and modeled T. The proposed method was applied to long-term EC measurements collected above a Mediterranean tree-grass ecosystem. Estimated E_s agreed with independent lysimeter measurements ($r = 0.69$). They also agreed with other partitioning methods derived from similarity theory and conditional sampling applied to turbulence measurements. These similarity schemes appeared to be sensitive to different χ parameterization. Measured E_s was underestimated by 30% when χ was assumed constant (= 0.8). Diel and seasonal χ patterns were characterized in response to soil dryness. A surprising result was a large E_s/ET throughout the seasons. The robustness of the results provides a new perspective on EC ET partitioning, which can be utilized across a wide range of climates and biomes.

1. Introduction

The role of plants in mediating the hydrological cycle at different spatial and temporal scales is rarely in dispute as evidenced by a number of reviews discussed elsewhere (i.e., Katul et al., 2012). Above land surfaces, water vapor exchange between the biosphere and atmosphere is mostly in the form of evapotranspiration (ET), an aggregated process consisting of transpiration from the plant (T) and evaporation from the soil and/or other wet surfaces (E_s). The relative contribution of these two components to ET remains a subject of inquiry and active research (Schlesinger & Jasechko, 2014). Recently, Wei et al. (2017) highlighted that current global mean T/ET estimates are largely uncertain, varying from 24% to 90% depending upon the method used for ET partitioning. Unsurprisingly, similar ranges can be explained at the local scale by ecosystem heterogeneities, fractional vegetation cover, and hydrological states of the ecosystem (Berkelhammer et al., 2016). Berkelhammer et al. (2016) observed a lack of consistent trend in the time series of T/ET, suggesting that E_s and T are, to some extent, tightly coupled. Scott and Biederman (2017) showed that T/ET is seasonal in arid sites and might vary from 23% to almost 60% due to frequency and timing of rainy days and the degree of vegetation cover. Using carbonyl sulfide measurements, Wehr et al. (2017) reported that E_s peaked during drought conditions with a contribution of up to 40% of the total ET. Air temperature was suggested as a primary factor explaining this pattern. Using stable oxygen isotopic measurements, Dubbert et al. (2014) showed that even though E_s was suppressed by vegetation, it was a large contributor to total ET during the growing season. These contrasting results might reflect both uncertainties resulting from the method used for ET partitioning (many are scale-dependent), the vegetation spatial distribution on the land surface, the soil type and soil moisture state, and the differential sensitivities of T and E_s to their respective driving forces. The need for a comprehensive analysis of ET components with

standardized methods that facilitate evaluation at the required spatial and temporal scales is becoming urgent (Fisher et al., 2017).

The partitioning of ET into E_s and T remains challenging due to several limitations and uncertainties of the current measurement techniques. With the constellation of eddy covariance (EC) flux sites networks, ET is available across many biomes and ecosystem types (Baldocchi et al., 2001). Relative to the widely used CO_2 flux partitioning methods that interpret both gross photosynthesis (P_h) and respiration from the net CO_2 fluxes (Lasslop et al., 2010; Reichstein et al., 2005), disentangling EC water fluxes remains challenging due to the limited ability to separately constrain T and E_s. For example, in the absence of photosynthetically active radiation, net CO_2 fluxes reflect ecosystem respiration rates thereby allowing nighttime EC measurements to be used to infer daytime respiration (but subject to many conditions and qualifications). However, in the case of water vapor fluxes, nighttime transpiration and evaporation can persist and often comprise up to 10% of daytime ET (de Dios et al., 2015; Novick et al., 2009).

Regardless of the methodological differences, existing EC-based approaches exploit correlations between CO_2 and water vapor exchange rates premised on the fact that during daytime, P_h and T follow similar pathways at the leaf scale. A case in point is the recent work by Zhou et al. (2016) who developed an ET partitioning strategy based on the concept of underlying water-use efficiency (uWUE; the P_h to ET ratio normalized by the root square of vapor pressure deficit [VPD]). Primary assumptions of the method are that (i) uWUE is constant over time and (ii) it can be retrieved from the net EC fluxes whenever the influence of E_s is minor and ET ≈ T. Given the increasing evidence that E_s is rarely negligible and that uWUE is not an *intrinsic* property of plants, such partitioning method might not be viable in arid ecosystems (Dubbert et al., 2014; Perez-Priego et al., 2017; Scott & Biederman, 2017). Unlike the method proposed by Zhou et al. (2016) that forces the intercept of the linear fit between $P_h\sqrt{VPD}$ and ET through the origin (ET = 0 when P_h = 0), Scott and Biederman (2017) found that the intercept between P_h and ET may be used in deriving E_s for water-limited sites. They showed that the intercept followed a seasonal pattern related to leaf area index and soil moisture conditions. Note that $\frac{P_h}{ET}$ represents the ecosystem level WUE, while the form $\frac{P_h}{ET}\sqrt{VPD}$ (inherited from optimal approaches; Hari et al., 2000; Katul et al., 2009; Medlyn et al., 2011) is alternatively used to express the *intrinsic* WUE. It is well known that ecosystem and whole-plant level WUE is highly dynamic and varies not solely in response to the evaporative demand but on a combination of physiological (Reichstein et al., 2003; Villalobos et al., 2012) and/or structural properties of the vegetation (Beer et al., 2009; Migliavacca et al., 2009). Even at the leaf scale, WUE varies with a number of environmental factors and physiological parameters as discussed elsewhere (Katul et al., 2010; Prentice et al., 2011).

Alternatively, the flux variance similarity (FVS) method employs a combination of turbulence scaling arguments and prior information of WUE, typically from leaf observations, to numerically solve water fluxes from high-frequency EC data (Scanlon & Kustas, 2010; Scanlon & Sahu, 2008). Although the method has been successfully applied to different ecosystem types (Scanlon & Kustas, 2010; Sulman et al., 2016; Wang et al., 2016), the accuracy of the method remains dependent on prior knowledge of plant WUE (Anderson et al., 2017). Also, the method assumes that the turbulent Schmidt numbers for CO_2 and water vapor are identical (Reynolds analogy), which may be questionable in nonideal meteorological conditions due to variability in sources and sinks near the ground and dissimilarity in entrainment fluxes.

From a physiological perspective, stomatal control of χ (the *internal* to ambient CO_2) and thus WUE is a cornerstone concept for water partitioning strategy. Stomatal behavior rests on observed relations between stomatal conductance, photosynthesis, and their environmental dependencies (Ball et al., 1987; Jarvis & McNaughton, 1986; Leuning, 1995; Wong et al., 1979). However, model parameters represent certain (typically favorable) situations but cannot interpret the underlying mechanisms leading stomata to functionally adapt and behave differently under contrasting conditions (Buckley, 2017). Based on the long-standing Cowan's hypothesis of the coupled plant carbon-water economies, an optimal stomatal behavior is predicted from the notion that plants maximize carbon gain for a given amount of available water (Cowan & Farquhar, 1977). Unlike empirical approaches, this optimality-based approach assumes that intrinsic properties and adaptive mechanisms can be described from a general hypothesis not rooted in a particular data set or species (Prentice et al., 2014). As supported by a comprehensive global $\delta^{13}C$ data set, the χ, a key aspect of WUE, can be described from the aforementioned optimality principles (Wang et al., 2017). Moreover, responses of

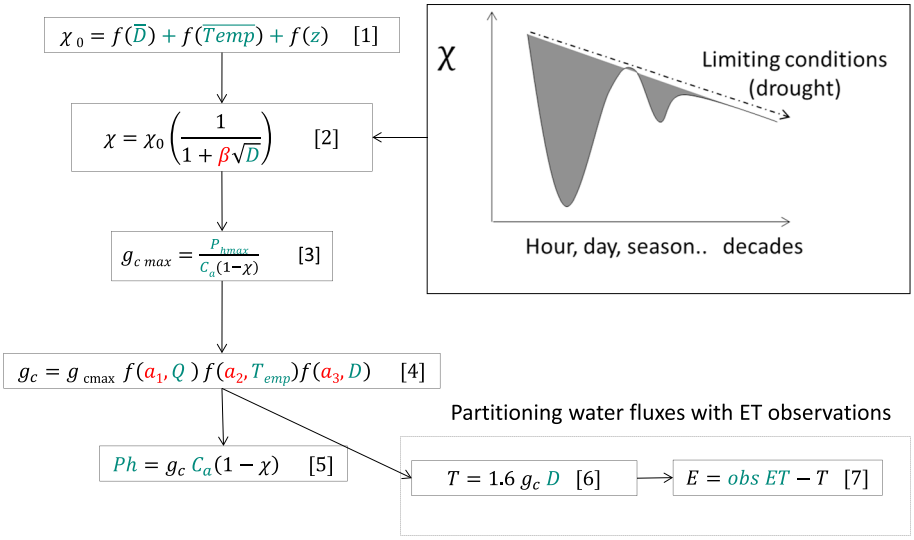

Figure 1. Conceptual workflow of the evapotranspiration (ET) water flux-partitioning approach. While the four model parameters (a_1, a_2, a_3, and β) are depicted in red color, the main variables used are represented in green color (equations (1)–(4)). Those include vapor pressure deficit (D), air temperature (T_{emp}), elevation (Z), and photosynthetic active radiation (Q). P_{hmax} stands for the maximum photosynthetic rate (P_h) observed over a 5-day window and estimated from the ninetieth percentile of the data. Optimal estimates of transpiration rates (T) are determined from the modeled g_c (for water vapor) according to equation (6). Evaporation is then calculated as the residual between the observed ET and estimates of T (equation (7)). A full description of the equations is provided throughout the text.

plants to elevated atmospheric CO_2, salinity, temperature, nutrient amendments, droughts, and other environmental controls have been acceptably reproduced from the aforementioned optimality arguments (Katul et al., 2010; Manzoni et al., 2013; Palmroth et al., 2013; Volpe et al., 2011; Way et al., 2011).

The underlying motivation of this study is to predict WUE so as to derive optimal T estimates thereby allowing partitioning of EC-based ET. Subsequently, ecosystem level E_s can be determined as a residual between T and ET. The challenges are, however, to test whether this approach applies to the temporal (i.e., diurnal variation) and spatial (from leaf to the canopy) scales as resolved by EC fluxes. Furthermore, the influence of the boundary layer conductance has been largely disregarded by optimal stomatal models, which have been developed by assuming that leaves are perfectly aerodynamically coupled, and it requires further consideration (Buckley et al., 2017). Hence, the specific goals here are twofold:

1) Develop a physiologically based EC water flux-partitioning scheme based on optimality principles, and
2) Evaluate the interplay between T and E_s across different environmental and climatic conditions.

A dedicated experiment in a Mediterranean tree-grass savanna ecosystem fully equipped with EC measurements along with independent lysimeter estimates of E_s described elsewhere (Perez-Priego et al., 2017) is used. Estimates of modeled WUE are used in the FVS (Scanlon & Kustas, 2012; Scanlon & Sahu, 2008) to predict T and E_s and to benchmark the method proposed here against different WUE parameterization schemes and assumptions.

2. Material and Methods

2.1. Model Development

The water flux-partitioning approach includes the following considerations and assumptions:

(1) An expression derived from the optimality theory is used to determine a site-specific long-term effective internal leaf-to-ambient CO_2 mixing ratio at the canopy scale (hereafter χ_o; equation (1) in Figure 1; Wang et al., 2017). This effective χ_o is to be interpreted here within the context of a *big leaf* representation and considered as the basis to solve for the canopy stomatal conductance (g_c) control of the exchange rates of P_h and T (equation (1)–(7) in Figure 1).

(2) The computed χ_o accommodates short-term kinetic adjustments (i.e., hours and seasons; equation (2) in Figure 1). There is some evidence that canopy-scale χ derived from ecosystem fluxes might exhibit diel patterns in response to variations in ambient vapor pressure deficit (Tan et al., 2017), which also agree with leaf-level observations (Fites & Teskey, 1988; James & Gifford, 1983; Jones, 1998; Katul et al., 2009). Different mathematical forms describing the dependence of χ with vapor pressure deficit can be found elsewhere (Katul et al., 2000; Leuning, 1990; Medlyn et al., 2011; Prentice et al., 2014).
(3) Short-term χ variations can be considered as part of the plant optimization problem and without the need of ignoring the boundary layer conductance influence.
(4) Environmental dependencies of g_c, represented by a Jarvis type formulation, are constrained in accordance with the inferred EC P_h pattern (equation (1)–(5)). Optimality theory is traditionally used for predicting g_c (Katul et al., 2010) when the physiological/photosynthetic properties of the plants are known. However, it is to be noted that we derive optimal predictions of χ while g_c is solved from its close relation with inferred P_h and their environmental dependencies. To this end, the Jarvis model is selected only to link environmental parameters to g_c (and other models can be used as well) without requiring the photosynthetic parameters. This data-model based approach provides stomatal conductance estimates (for water vapor) that eventually can be used to infer optimal T (equation (6)). Finally, E_s is calculated as the residual between T estimates and ET observed by EC (equation (7)).
(5) Finding the numerical solution for the optimal set of parameters (β, a_1, a_2, and a_3) in equations (2) and (4) over a 5-day window that satisfies the objective function of minimizing T while maximizing P_h is posed here as part of the parameter optimization problem. This approach is in contrast to the original problem of solving the optimal pattern of stomatal aperture variation in time for prescribed time-varying environmental parameters. Instead, the model parameters (β, a_1, a_2, and a_3) are to be determined in a manner that minimizes T while maximizing P_h over the overall period of interest. The way we apply this premise to EC data as well as the estimation of the parameters is further detailed throughout this section.

The approach commences from P_h—the only known stomatal flux that can be inferred from EC data (Reichstein et al., 2005)—assumed to be represented as follows:

$$P_h = \rho_a g_c C_a (1 - \chi), \tag{8}$$

(note that equations (1)–(7) are reported in Figure 1) where P_h is a molar flux density (μmol $CO_2 \cdot m^{-2} \cdot s^{-1}$), g_c is the canopy stomatal conductance (m/s), C_a is the ambient CO_2 mixing ratio (μmol CO_2/mol), and ρ_a is the molar air density (mol/m^3). A list of symbols is given in Table 1.

According to equation (8), the two unknowns are χ and g_c. There is now sufficient evidence to argue that χ_o may be described by a general function, at least for C_3 plants (Prentice et al., 2011; Wang et al., 2014, 2017). This justifies lumping mixed vegetation surfaces (e.g., tree-grass ecosystem) as a *big-leaf* provided their photosynthetic machinery is C_3. The least-cost optimality hypothesis, firstly formulated by Wright et al. (2003) and further developed by Prentice et al. (2014), predicts that χ tends to increase with increasing temperature (*Temp*) and to decrease with increasing atmospheric vapor pressure deficit (*D*) and elevation (*Z*). Such dependencies have been quantitatively derived by Wang et al. (2017) and are given by

$$\ln\left(\frac{\chi_o}{1-\chi_o}\right) = 0.0545\left(\overline{Temp} - 25\right) - 0.25\ln\overline{D} - 0.0815Z + C. \tag{9}$$

The overlined characters ($\overline{Temp}$ and $\overline{D}$) are used to denote growing season average daytime values, and C is a coefficient fixed to 1.189 for C_3 plants according to Wang et al. (2017). Given that equation (9) predicts a long-term *optimal* value (χ_o), which might mask short-term responses, here we further hypothesize that χ decays over the course of a day with increasing D (Mortazavi et al., 2005; Tan et al., 2017). For example, a simplified leaf-level optimality approach (for Rubisco-limited photosynthesis of C3 plants) predicts short-term variations in $\chi \approx 1 - \sqrt{\frac{D}{C_a}a\lambda}$, provided the marginal water use efficiency λ varies with atmospheric CO_2 over long timescales (Katul et al., 2010). Because of these findings, a diel sensitivity factor $\left(1/\left(1+\beta\sqrt{D}\right)\right)$ is used to describe diurnal variations of χ that are consistent with several leaf-level optimization (equation (2)). Note that β (or λ) is the intrinsic WUE and measures "the carbon cost of water," which can be found elsewhere as b_1 or ξ (Lin et al., 2015; Medlyn et al., 2011; Prentice et al., 2014). Here β is used to denote a diel-response parameter

Table 1
List of Variables

Symbol	Units	Description
P_h	$mmol \cdot m^{-2} \cdot s^{-1}$	Gross photosynthetic flux
T	$mmol \cdot m^{-2} \cdot s^{-1}$	Plant transpiration rate
ET	$mmol \cdot m^{-2} \cdot s^{-2}$	Evapotranspiration rate
E_s	$mmol \cdot m^{-2} \cdot s^{-3}$	Evaporation rate from the soil and/or other wet surfaces
χ	~	Internal to ambient CO_2 concentration to be numerically solved
χ_o	~	Long-term effective χ derived from its environmental dependences
R_n	W/m^2	Net Radiation
G	W/m^2	Ground heat flux
LE	W/m^2	Latent heat flux
H	W/m^2	Sensible heat flux
WUE	mmol/mmol	Water use efficiency
g_x^z	m/s	Conductance. The subscript X can stand for bulk surface conductance (g_{bulk}), canopy stomatal conductance (g_c), or aerodynamic conductance (g_a). The latter calculated as the sum of the resistances to momentum transfer (g_{aM}) and to heat transfer (g_b). The subscript z expresses whether the conductance term is expressed for heat (H), CO_2 (no symbol is used), or water vapor (W). Note that g can be expressed in units of mmol $CO_2 \cdot m^{-2} \cdot s^{-1}$ or mmol $H_2O \cdot m^{-2} \cdot s^{-1}$ (g^W) by considering changes in ρ and the respective diffusion coefficients
D	kPa	Vapor pressure deficit
c_p	$J \cdot kg^{-1} \cdot K^{-1}$	Specific heat capacity
ρ_a	mol/m^3	Molar air density
β	$kPa^{-0.5}$	Diel-response parameter denoting the *carbon cost of water* to be numerically solved
a_1, a_2, a_3	~	Fitting parameters
Q	$mmol \cdot m^{-2} \cdot s^{-1}$	Photosynthetic active radiation
T_{emp}	K	Air temperature
Z	km	Altitude

Note. The overlined character in D and T_{emp} can be is used to denote growing season average daytime values.

that is optimized over a 5-day window. Expectations are that a constant χ is achieved when β or λ are small (no diel variations). On the contrary, a more accentuated decline of χ would follow during soil moisture deficit to support an increasing photosynthetic capacity (Wright et al., 2003) and eventually the expected increased WUE (Palmroth et al., 2013; Villalobos et al., 2012). This agrees with evidence that short-term χ derived from leaf gas-exchange observations tend to decline when g_s limits P_h while being relatively constant under optimum conditions (see Figure S1 in the supporting information; see also Figure 4 in Katul et al., 2009). Because β (or λ) is unknown, this parameter is retained in the parameter optimization to be discussed.

When stomata operate optimally, it is reasonable in a plant optimization scheme to infer a maximum g_c (g_{max}) when the daily maximum EC-derived P_h (Ph_{max}) is observed—normally over the mornings at low D. According to Jarvis (1976), we interpret the dynamic change of g_c by scaling the derived g_{max} through a series of multiplicative functions defining stomata responses to environmental conditions (i.e., photosynthetically active radiation, Q; air temperature, T_{emp}; and vapor pressure deficit, D):

$$g_c = g(Q) f(T_{emp}) f(D), \text{where} \tag{10}$$

$$g(Q) = \frac{g\,\max Q}{Q + a_1}, \tag{11}$$

$$f(T_{emp}) = b_1 (T_{emp} - T_{min}) (T_{max} - T_{emp})^{b_2}, \tag{12}$$

with b_1 and b_2 derived as

$$b_1 = \frac{1}{(a_2 - T_{min})(T_{max} - a_2)^{b_2}}, \tag{12.1}$$

$$b_2 = \frac{(T_{max} - a_2)}{(T_{max} - T_{min})}, \tag{12.2}$$

$$f(D) = \exp(-a_3 D), \tag{13}$$

the parameter a_2 denotes the optimum temperature and T_{max} and T_{min} the highest and lowest temperatures set to 0 and 40 °C, respectively. Other forms to equation (13) can be used that are anchored to outcomes of stomatal optimization (e.g., see equation (8) in Katul et al., 2010, and others—Dewar et al., 2018). Here D stands for leaf-to-air vapor pressure deficit and is calculated by accounting for plant temperature, a better driving factor of stomata conductance (Perez-Priego, Lopez-Ballesteros, et al., 2015). Because plant temperature is rarely measured, we define a *bulk* surface temperature as $T_{bulk} = Hr_a/c_p\rho + T_{emp}$ as a proxy for plant temperature where H is the sensible heat flux (H) measured by the EC system, $c_p\rho$ is the volumetric heat capacity, and r_a is the bulk aerodynamic boundary layer resistance. Changes in heat storage are disregarded. To account for the influence of the canopy boundary layer, g_c in equation (8) is replaced by the "bulk" surface conductance (g_{bulk}), which is calculated as

$$\frac{1}{g_{bulk}} = \frac{1}{\frac{1}{g_c} + \frac{1}{g_a}}, \tag{14}$$

where g_a (or its inverse resistance, r_a) is characterized in terms of aerodynamic resistance to momentum transfer (g_{aM}) and to heat transfer (g_{bH}) and computed according to Monteith and Unsworth (2013) as $\frac{1}{g_a} = \frac{1}{g_{aM}} + \frac{1}{g_{bH}} = \frac{u}{u_*^2} + 6.2u_*^{-0.67}$ (equations (17.5) and (17.8)). Based on molecular diffusivities, g_c to water vapor (g_c^w) is approximated as $g_c^w \approx 1.6g_c$, being 1.6 the diffusivity factor between CO_2 and water vapor. Similarly, the diffusivities causes between g_b for heat (g_{bH}), CO_2 (g_b), and water vapor (g_b^w) were calculated according to Hicks et al. (1987). Therefore, $r_b = N\left(\frac{Sc}{Pr}\right)^n r_{bH}$ and $r_b^w = N\left(\frac{Scw}{Pr}\right)^n r_{bH}$, where $N = 1$ for amphistomatous leaves or 2 for hypostomatous leaves, Sc is the molecular Schmidt number for CO_2 (≈ 1.05), and Scw is the molecular Schmidt number for water vapor (Scw ≈ 1.6 Sc), Pr is the molecular Prandtl number for air (≈0.71), and n is an empirical turbulence parameter (≈ 0.66). Here, it is assumed that mesophyll conductance is infinite and is therefore neglected. This assumption may be questionable as a number of studies have already suggested that mesophyll conductance can be restrictive during plant stress conditions—whether be they soil moisture or salt stress related (Dewar et al., 2018; Volpe et al., 2011). If mesophyll conductance limits photosynthesis, then β, a_1, a_2, and a_3 must be treated as effective as they will effectively *absorb* the mesophyll limitations during plant stress conditions. Hence, it will be difficult to provide a causal explanation to the increases in optimized β during plant stress conditions in relation to soil moisture only. However, this difficulty in parameter interpretation does not appreciably impact the sought-after goal of separating ET into its two constituent terms. Notwithstanding this parameter interpretation issue, g_c can be used to derive transpiration as follows:

$$T = \rho_a g_{bulk}^w \frac{D}{P_a}, \tag{15}$$

where P_a is the atmospheric pressure. Finally, E_s is derived from EC-measured ET and modeled T as shown in equation (7) in Figure 1.

2.2. Model Optimization

The four model parameters (β, a_1, a_2, and a_3 in equations (2)–(5)) were estimated using a multiconstraint Markov chain Monte Carlo as implemented in the Delayed Rejection Adaptive Metropolis algorithm of the A Flexible Modelling Environment for Inverse Modelling, Sensitivity, Identifiability and Monte Carlo Analysis package (R Development Core Team, 2010). As a novelty, the objective function is to find those numerical solutions that minimize not only the mismatch between observed and modeled P_h but also the unit cost of transpiration by introducing a conditional factor demand (Φ), which invokes the optimality hypothesis. Accordingly, the objective function is defined as

$$OF = \Sigma\left(\frac{Obs_i - Mod_i}{\varepsilon}\right)^2 / n + \overline{\Phi}, \tag{16}$$

where the first term denotes the mean sum of the square between observed (inferred) and modeled P_h, which are normalized by the flux measurement errors ($\mathcal{E}$, calculated as the variance of the covariance according to Finkelstein & Sims, 2001), and the second term the mean Φ defined as the integrated cost of transpiration (i.e., $\int T/\int P_h$) over a time period (5 days) normalized by a factor describing an optimal WUE_o.

The optimal WUE_o was calculated as $WUE_o = C_a(1-\chi_o)P_a/\left(1.6\overline{D}\right)$, which results from combining equations (8) and (15). C_a and P_a are fixed at 390 ppm and 96 kPa, respectively. In the optimization routine, we assume uninformative uniform priors of each parameter. The lower and upper bounds of the a_1, a_2, a_3, and β parameters were restricted to 0, 0, 10, and 0 and 400, 0.4, 30, and 1, respectively. The number of iterations was set to 20,000, and the first half of the chains was discarded. We updated the proposed distribution every 500 iterations. The Markov chain Monte Carlo calibration was performed on a daily basis using a 5-day moving window. This time period is consistent with the one used for daytime Net ecosystem CO_2 exchange (NEE) partitioning methods and is typically used to guarantee on one hand a good number of half-hourly data for the model fitting and on the other hand a window relatively small to catch the response of *T*/ET partitioning at short timescale (i.e., rain events or sudden increase of VPD that can regulate transpiration). For the optimization, only high-quality data were used: (i) quality flags of the CO_2 fluxes = 0 according to Mauder and Foken (2004); (ii) wind friction velocity threshold filtering criterion according to Perez-Priego et al. (2017); and (iii) no precipitation. To monitor the convergence of the Markov chain simulation toward the posterior distributions of parameters, we started three Markov chains from three random parameter sets generated by Latin hypercube sampling from the prior and checked that the Gelman diagnostic is smaller than 1.1 (Gelman & Shirley, 2011). While parameters were estimated from the best parameter fit, we sampled 100 parameter sets from the posterior distribution to propagate model uncertainties.

3. Data

3.1. Site Description

The model was tested using data from an experimental site located in a Mediterranean tree-grass savannah in Spain (39°56′25″N, 5°46′29″W; Majadas de Tietar, Caceres). The site is characterized by a mean annual temperature of 16 °C, mean annual precipitation of approx. 650 mm, falling mostly from November until May with prolonged dry summers. The vegetation is composed of a low-density tree cover (mostly *Quercus ilex* (L.), approx. 20 trees/ha, and mean diameter at breast height of 46.86 cm) and dominated by a herbaceous stratum during the growing season (Perez-Priego et al., 2017). The fractional cover of the herbaceous stratum with the three main functional plant forms (grasses, forbs, and legumes) varies seasonally according to their phenological status (Perez-Priego, Guan, et al., 2015), with important interannual variations related to the onset of the dry period. Overall, herbaceous stratum peaks around end of March with mean plant area index values of up to 2 m^2/m^2, achieves senescence by the end of May, and greens up by the fall after a long dry summer (Migliavacca et al., 2017). The soil is classified as an Abruptic Luvisol (IUSS Working Group WRB, 2015) and originates from Pliocene-Miocene alluvial deposits. The upper limit of the clay horizon is found at a depth between 30 and 100 cm. The texture in the upper horizons is sandy (80% sand, 9% clay, and 11% silt).

3.2. Instrumentation

3.2.1. EC, Lower Boundary-Controlled Lysimeters, and Ancillary Data

An EC system was operated for 3 years (2015–2017) at 15-m height (more detailed information can be found in Perez-Priego et al., 2017). Briefly, the set of instruments consisted of a sonic anemometer (Gill R3–50; Gill Instruments Limited, Lymington, UK) and an enclosed path infrared gas analyzer (LI-7200, LI-COR Biosciences Inc., Lincoln, NE, USA). A net radiometer was placed at the top of the tower (CNR4, Kipp&Zonen, Delft, Netherlands). EC raw data—including sonic temperature (K), the three-dimensional wind velocities (*u*, *v*, and *w* in m/s), and dry CO_2/H_2O mixing ratios—were collected at 20 Hz and processed with EddyPro version 5.2.0 (Fratini & Mauder, 2014). A detailed description of data processing, error determination, and quality check can be found in Perez-Priego et al. (2017). The EC tower was equipped with a hygrothermometer (Thies Clima, Göttingen, Germany) in a ventilated shelter to measure air temperature and humidity. Additionally, the incident photosynthetically active radiation (*Q*) was measured with a quantum sensor (PQS1 PAR Quantum Sensor, Kipp&Zonen, Delft, Netherlands). Net ecosystem CO_2 fluxes were gap-filled (Reichstein et al., 2005) and partitioned into gross photosynthesis (P_h) and ecosystem respiration using both nighttime (Reichstein et al., 2005) and daytime (Lasslop et al., 2010) partitioning implemented in the REddyProc 0.7-1 R package (Wutzler et al., 2018). For simplicity, we will refer nighttime and daytime partitioning methods as MR and GL, respectively. The normalized difference vegetation index (NDVI) was used as a descriptor of plant leaf development and extracted from the MODIS 16-day land surface reflectance data (MOD13Q1, at 3 × 3 pixel of 250-m spatial resolution centered at the EC tower).

Three PE-HD container weighable lysimeter stations (8-m^2 area and 2.5-m length) were installed underground at the different sites (open space covering the grass) spread out over the fetch of the EC tower. Each station contained two weighable lysimeters of the lower temperature- and tension-controlled (LBC) type. An undisturbed soil monolith of around 2,700 kg (under dry conditions) was packed into each lysimeter vessel using an original lysimeter soil retriever technique (Reth et al., 2007). This novel lysimeter type includes a lower-boundary-controlled system that facilitates control of both soil matrix tension and temperature to mirror the actual values in the surrounding soil. This provides accurate estimates of ET while minimizing soil disturbances. Briefly, the tension-controlled system consisted of 10 porous ceramic bars that connect the capillary system of the soil at the bottom of the lysimeter vessel to a pressure-regulated, airtight water tank. The air pressure inside the tank is regulated according to the actual soil matrix tension outside the station measured by a reference tensiometer (Tensio160, VKWA 100 Tipping counter, Umwelt-Geräte-Technik GmbH, Müncheberg, Germany). A heat exchanger system maintained the temperature at the bottom layer of the soil column equal to that of the surrounding soil. Each lysimeter vessel was made of a stainless steel cylinder with a cross-sectional area of 1.0 m^2 and 1.2-m depth and wrapped with a temperature-insulated sheet to keep natural temperature and tension gradients along the soil monolith profile. Soil moisture and temperature (UMP-1, Umwelt-Geräte-TechnikGmbH, Müncheberg, Germany) at 10, 30, 75, and 100 cm were measured inside each lysimeter.

A flat concrete surface at each station provides a robust basis for the weighing system. Every lysimeter vessel sits on a load triangle with three precision shear-stress cells (Model 3510, Stainless Steel Shear Beam Load Cell, VPG Transducers, Heilbronn, Germany) mounted on a stainless steel supporter. The load cells were previously calibrated with known mass and were able to sense variations of up to 10 g/m^2 ground surface. A tipping counter measured water seepage (VKWA100 Tipping counter, Umwelt-Geräte-Technik GmbH, Müncheberg, Germany). The lysimeter's weight was recorded every 1 min. Once correcting for changes in mass via the LBC system and excluding periods of water seepage and precipitation, evaporative loss (expressed as positive values), or mass gain by dew fall (expressed as negative values) were calculated then as the differences in mass from the previous time interval.

Calculated water fluxes were processed using a comprehensive data quality and assurance procedure. Briefly, fluxes were calculated using 15-min time intervals (F_i). A moving function ($|F_i - \text{median}(F_{i=1}^{i=15})|$/MAD) containing the median absolute deviation (MAD) of F_i was performed over 15 min to detect anomalies. Those values exceeding 1.5 were removed and excluded from calculations. For comparison with the EC data, calculated F_i within every half-hour were averaged and converted to water vapor molar fluxes (mmol $H_2O \cdot m^{-2} \cdot s^{-1}$). A second filter criterion used the MAD of calculated fluxes from the six lysimeters (F_{Lys}). Accordingly, data for which $|F_{Lys} - \text{median}(F_{Lys})|/\text{MAD} > 2$ were also flagged as an outlier. Finally, the ensemble of half-hourly unflagged F_{Lys} values was used to calculate the mean and the standard deviation, which were considered as an integrative quantity of the understory ET and its associated variability.

3.3. Model Evaluation and Benchmarking

For evaluation, E_s estimates derived from the model were compared against independent lysimeter observations during dry periods, when grass is already senescence and the observed ET by the lysimeter defines E_s. It is worth mentioning that the mismatches between EC-derived ET and independent estimates at this site are below an acceptable threshold (20%) during certain environmental conditions (i.e., turbulent mixing deficiencies and/or stable atmospheric stratification and high relative humidity) and that the Bowen ratio method (Twine et al., 2000) may be applied to the EC data to correct for the lack of energy balance closure (92%; Perez-Priego et al., 2017). We rejected corrections that lead to implausible values (i.e., corrected ET $>$ 2 times the observed ET). For those conditions and when quality flags of the ET fluxes = 0, the observed ET was considered as a good quality.

In addition, the optimized WUE from the model was used as an input to the FVS method schemes to explore its validity (Scanlon & Kustas, 2012; Scanlon & Sahu, 2008). Given that FVS has recently emerged as one of the promising water flux partitioning methods (Skaggs et al., 2018), the degree of accuracy of the FVS method associated with different WUE parameterization schemes is further evaluated here.

Briefly, the FVS method relies on the assumption that *stomatal* and *nonstomatal* turbulent fluxes conform to flux-variance similarity. Under this theoretical premise, an analytical approach is built such that stomatal and

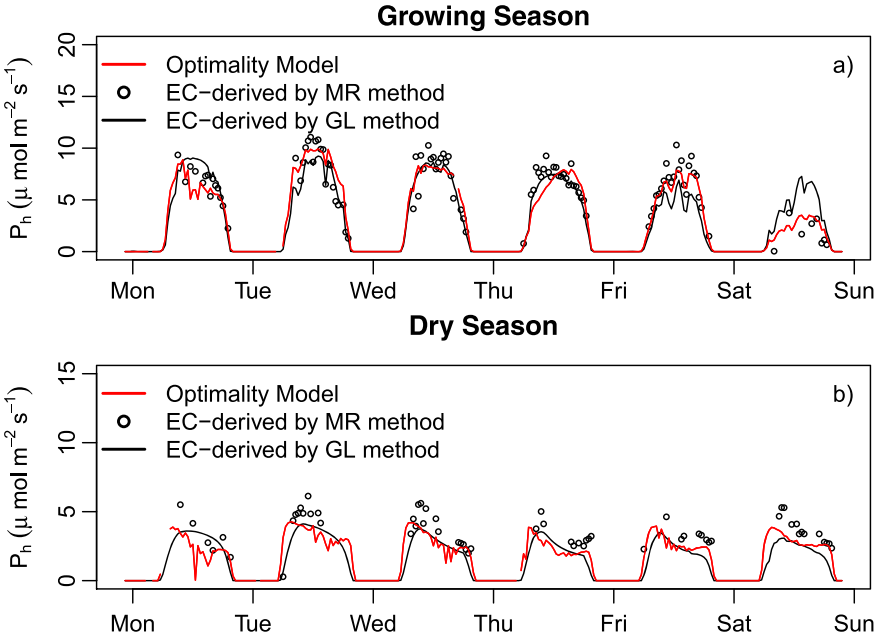

Figure 2. Diurnal variations of gross photosynthesis (P_h) inferred from the eddy covariance (EC) CO_2 fluxes using the approaches described in Reichstein et al. (2005; MR method, circles) and Lasslop et al. (2010; GL method, black solid line) modeled P_h (red solid line) in two representative periods: (a) growing (top) and (b) dry (bottom) seasons.

nonstomatal turbulent exchange results in perfect correlations between high-frequency measurements of water vapor and CO_2 concentrations (i.e., exchange associated with P_h and T results in a correlation coefficient of -1 between the concentrations, while exchange associated with E_s and respiration results in a correlation coefficient of +1 between the concentrations). This correlation-based flux partitioning approach only requires high-frequency time series of CO_2 and water vapor concentrations derived from conventional EC instrumentation and prior information of plant WUE. More complete details about this method can be found in a number of prior publications (Palatella et al., 2014; Scanlon & Kustas, 2012; Scanlon & Sahu, 2008; Skaggs et al., 2018).

Accordingly, 20-Hz EC data series despiked and corrected for CO_2 and water vapor lags were used to compute the required inputs including standard deviation of the water vapor and CO_2 fluctuations, as well as the correlation between water vapor and CO_2 and their respective fluxes. The improved numerical solution of FVS suggested by Palatella et al. (2014) and implemented in a Matlab routine was used to derive both T and E_s flux components. The FVS partitioning procedure has been recently implemented in an open source Python module (Skaggs et al., 2018).

Particularly, three different WUE parameterization schemes were compared:

1. FVS optm: WUE estimates were directly derived from the optimality model.
2. FVS seasonal: Here we fixed the β parameter as 0 (equation (2)) and assume $\chi = \chi_0$. Accordingly, χ is only assumed to vary over the season.
3. FVS fixed: here we fixed χ as a constant value. This approach is based on the assumption that χ may be relatively constant when stomata operate optimally (Ball & Berry, 1982; Wong et al., 1979). Former studies fixed a relatively stable value of 0.8 for C3 plants (Norman, 1982). Although more recent studies have shown this ratio to fall between ±35% (Hetherington & Woodward, 2003), here we used a fixed value of 0.8.

4. Results

4.1. Model Performance and Physiological Patterns

Figure 2 illustrates the diel patterns of modeled and inferred P_h during a week of two representative (a) growing and (b) dry periods in 2017. As a characteristic of Mediterranean ecosystems, pronounced decreases of P_h over the afternoons were well reproduced, particularly over the dry period when stomata reduce the gas

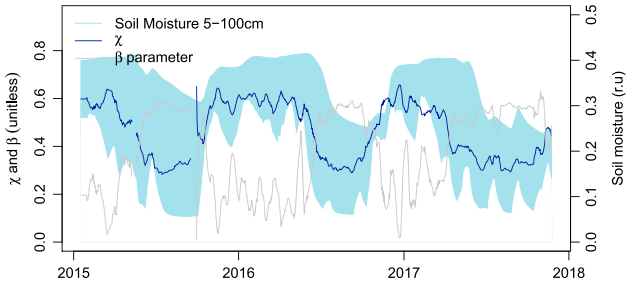

Figure 3. Seasonal variation of the ratio of *internal* to ambient CO_2 ratio (C_i/C_a and referred to as χ over the text; dark blue line), the β parameter that relates to the carbon cost of water and soil moisture profile (gray line). The upper bound of the blue polygon represents the soil moisture at 100-cm depth, while the lower bound the moisture at the shallow layer (5-cm depth). Lines represent a 14-day moving average.

exchange in response to high *D*, which led to more accentuated asymmetric diel patterns as compared to the wet season. The model performance was generally acceptable with good agreement between modeled P_h and inferred P_h by MR partitioning algorithm (slope = 1.1, r^2 = 0.73, MAE = 1.64 μmol $CO_2 \cdot m^{-2} \cdot s^{-1}$; Figure S2a) as well as by the GL method during the 3-year study (slope = 1.1, r^2 = 0.77, MAE = 1.57 μmol $CO_2 \cdot m^{-2} \cdot s^{-1}$; Figure S2b). The Φ term, the transpiration cost term in the multiconstraint cost function (equation (16)), followed a dynamic seasonal trend peaking throughout the dry summer with the lowest values over the winter. Φ ranged between 0% and 35% of the root mean square error (see Figure S3). Residuals of the models were not correlated with Φ. The Gelman diagnostic values were lower than 1.1 in most cases, which indicates that the convergence of multiple Markov chain Monte Carlo chains runs independently of the initial parameters. Generally, the model was sensitive to changes in the climatic forcing (i.e., light, stability conditions, temperature, and humidity) as shown by the variability among the days presented in both periods. The P_h inferred from EC data by either MR or GL partitioning methods should not be considered as an observation but an estimate. Given that MR partitioning method entails fewer modeling assumptions than GL partitioning (Wutzler et al., 2018), we considered EC P_h estimates by MR method as the reference to constraint the optimal model. Note that the MR method relies exclusively on the assumption that the temperature response function of nighttime net CO_2 fluxes can be used to predict daytime respiration, while the GL method estimates P_h through a fitting function that accounts for the combined effects of radiation and VPD as well as the temperature response of respiration (see Lasslop et al., 2010; Reichstein et al., 2005; Wutzler et al., 2018). The influence of the boundary layer resistance was accounted for in the optimality model, which explains the observed fluctuations of model estimates (see differences between modeled P_h and those by GL method; Figure 2b).

The model showed the lowest χ values during the summer drought when the cost of transpiration was high ($\beta \rightarrow 1$) due to a perceptible soil moisture deficit. Conversely, χ was relatively stable and closer to χ_o during the growing-wet season ($\beta \rightarrow 0$; Figure 3). This characteristic trend illustrates the dynamic physiological responses under optimum and limiting conditions; while χ holds relatively constant over the growing-wet period, with values around 0.6, a more accentuated χ drawdown was observed during the dry period when g_c was typically reduced to offset the increasing cost of transpiration. A fully detailed illustration of the dynamic between χ and g_c along with its close relation with P_h over a drying down period is provided in Figure S4.

The observed seasonal trend of χ was associated with soil moisture variations consistent with a large corpus of data and model results linking plant hydraulics to photosynthesis (Katul et al., 2003). As expected, the increase in *D* and soil moisture deficit imposed a χ drawdown, which was partially modulated by the optimized β parameter. According to the optimality, the derived analytical expression (equation (2)) predicted that χ approached its optimum at low transpiration cost values (i.e., low β values). On the contrary, the increase in both *D* and soil moisture deficits imposed a higher transpiration cost that was accompanied by a reduction of both g_c and χ. This pattern can be understood as a synchronized mechanism to support a higher photosynthetic capacity while reducing transpiration. Accordingly, a higher adjustment of β over the dry periods always entails an increase in WUE (see Figure S5). While variations in β have been historically used as evidence against stomata operating optimally (Fites & Teskey, 1988), it is imperative to note here that β is assumed constant over a 5-day window. This period is much longer than the timescale over which stomatal aperture opens and closes. Furthermore, it was shown elsewhere that slow variations in β do not alter the optimality predictions of g_c and χ (Manzoni et al., 2013).

4.2. Model Evaluation

Diel patterns of soil evaporation (E_s) estimated from the model followed the lysimeter measurements closely during the dry period. Overall, a diminishing diurnal pattern of E_s with increasing drought is usually observed over the periods (Figure 4a). E_s peaked around midday with values of up to 5 mmol $\cdot m^{-2} \cdot s^{-1}$ during the transition of the wet-to-dry season to the lowest values around 1 mmol $\cdot m^{-2} \cdot s^{-1}$ during severe drought

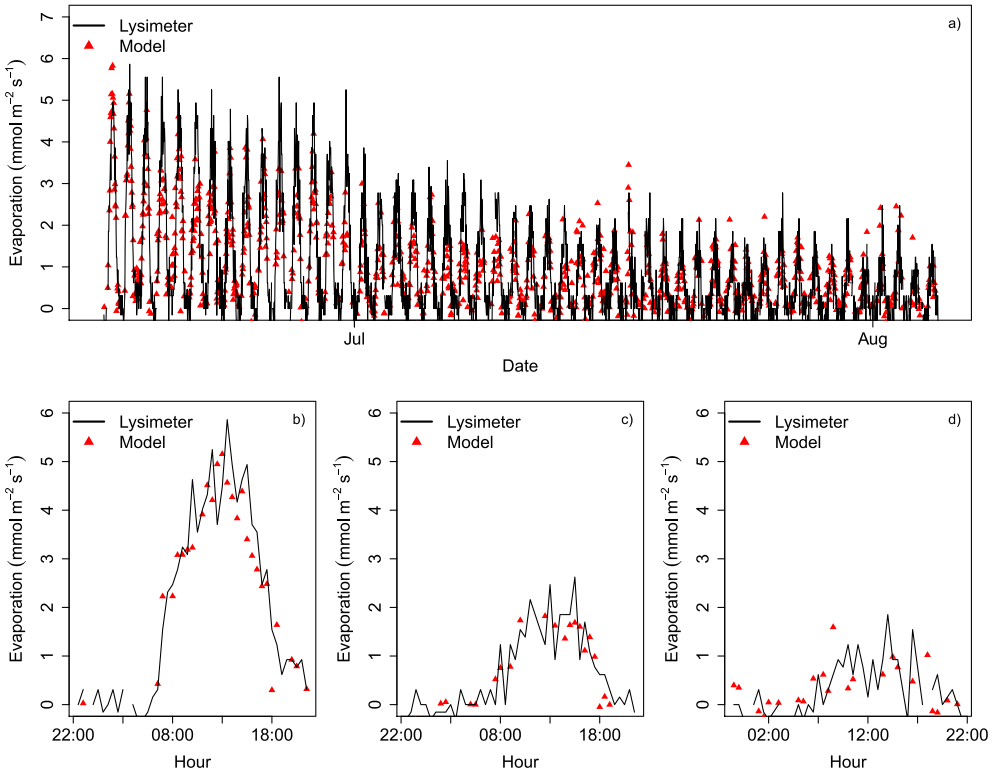

Figure 4. Diurnal time courses of both modeled (red triangles) and observed E_s using the lysimeters (black line) throughout (a) a drying-down period during a summer period in 2015 (from 16 June to 6 August), (b) 17 June, (c) 12 July, and (d) 5 August. Both showed a close agreement over the drying-down period when grass was already senescence, and evapotranspiration (ET) rates by lysimeters was mostly driven by soil evaporation.

conditions (Figures 4b–4d), when E_s flatted out over the course of the day (Figure 4d). The agreement between E_s rate estimates from the model against independent observations (i.e., lysimeter) was acceptable for the whole dry periods within the 3 years (MAE = 0.49 mmol · m^{-2} · s^{-1}, slope = 0.95, r = 0.69; see Figure S6).

Mean diel patterns of plant transpiration both derived from the model and using the FVS optm method followed closely each other during the dry period (Figures 5a and 5b). However, a clear discrepancy was found between transpiration estimates by the optimality model and FVS optm and those by FVS season and FVS fixed. This suggests that transpiration rates are systematically overestimated whenever neither mid-term nor short-term kinetic adjustments of χ in response to water stress are accounted for in models. Results revealed that transpiration is overestimated by 30% when WUE is parameterized with a constant value of χ = 0.8 (FVS fixed against FVS optm, MAE = 0.48 mmol · m^{-2} · s^{-1}; Figure 6a). Discrepancies were reduced when the parameterization scheme allowed χ to vary throughout the season (FVS season against FVS optm, MAE = 0.29 mmol · m^{-2} · s^{-1}; Figure 6b).

The seasonal time courses of T and E_s were dynamic, peaking around 1–3 mmol · m^{-2} · s^{-1} over the growing-wet season and declining to its lowest values during the dry and winter periods (Figure 7a). E_s and T followed similar seasonal patterns over the transition of the growing season when evaporation was mostly driven by available energy. However, E_s declined earlier than T during the drying-down period with the absence of precipitation (Figure 7b). Notably, E_s was inhibited when the shallow layer dried out while trees withdrew water from the wet deeper soil. E_s estimates followed much closer the observations by the lysimeters during the dry period as compared to the growing season when the differences were attributed to grass transpiration.

4.3. ET Component Fluxes and Drivers

Estimates of E_s were strongly associated with changes in soil moisture, which eventually were associated with an increased vegetation cover, and in particular the herbaceous stratum. Surprisingly, the fractional E_s/ET

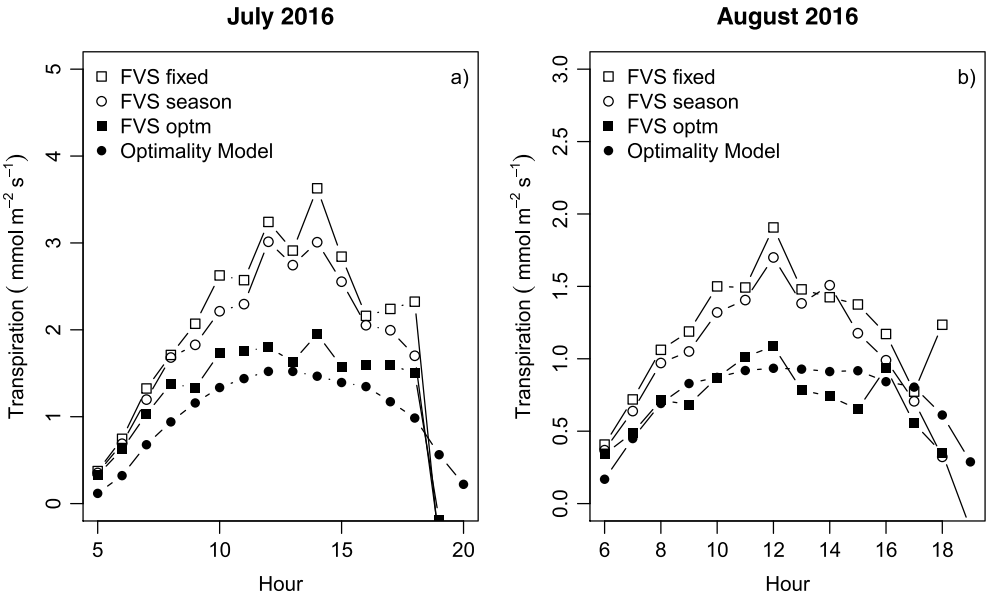

Figure 5. Monthly mean diurnal time courses of transpiration for (a) July 2016 and (b) August 2016 estimated by the optimal model (black circles), flux variance similarity (FVS)-optm (black squares), FVS-fixed (white squares), and FVS-season (white circles).

increased exponentially with NDVI, suggesting that E_s was not suppressed by vegetation, particularly during the dry period (Figure 8). The observed spread of the data when E_s/ET tends to be flat at high NDVI values could be explained by sporadic precipitation. A sustained pattern of E_s/ET values around 0.6–0.8 was observed while NDVI spanned between 0.4 and 0.7 values (Figure 8a). Although a decrease in soil moisture of the upper soil was correlated with NDVI (Figure 8b), high E_s/ET values were sustained by the wet deeper soil (1 m). Certainly, only an abrupt decrease of E_s/ET around the lowest NDVI values (0.4) was observed whenever the deeper soil dried out.

Surprisingly, the role of E_s was not negligible either during the severe summer drought, which was supported by lysimeter measurements, or during the growing periods. Indeed, it contributed to a large portion of the total ET. The highest E_s/ET values were found during the growing period (approx. 80%), which suggests that the available energy to evaporate water from the soil is not a limiting factor regardless of the full

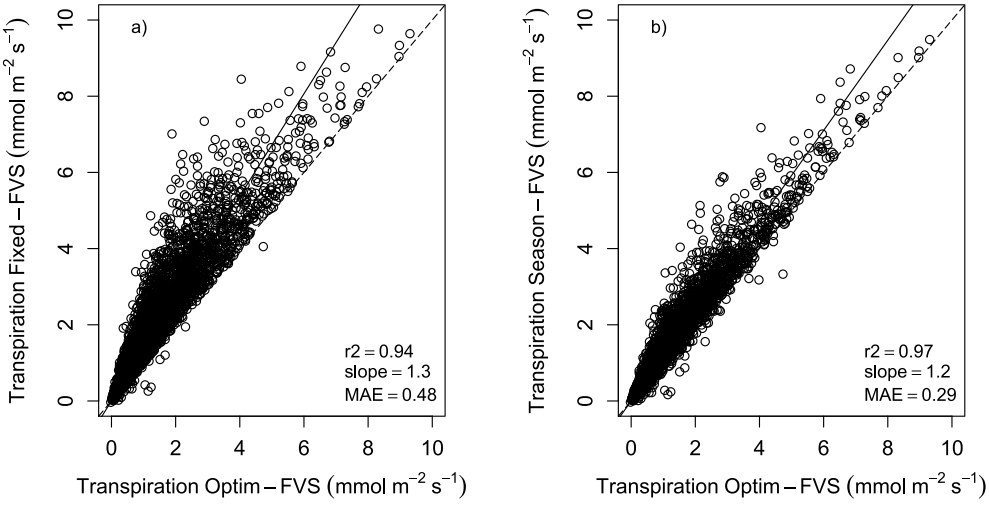

Figure 6. Comparison between transpiration estimates between flux variance similarity (FVS)-optm and (a) Fixed-FVS and (b) Season-FVS. Results from the statistical analysis are included.

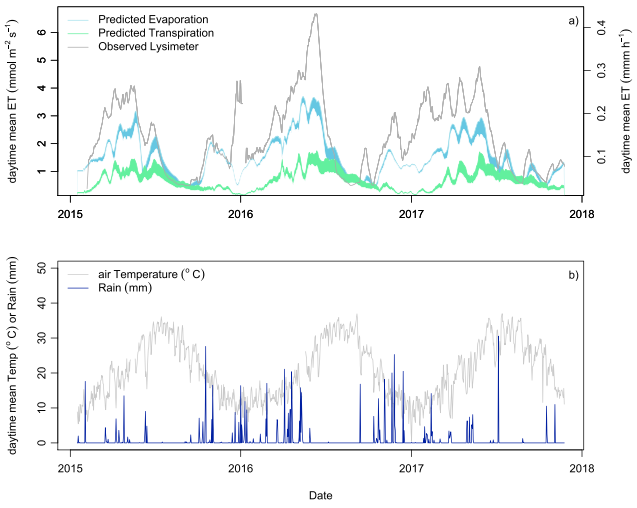

Figure 7. Seasonal variations of (a) modeled stand transpiration (*T*, including grass and tree contributions, green area) and derived evaporation (E_s, blue area) and independent evapotranspiration (ET) observations with lysimeters (gray line), and (b) air temperature (gray color) and precipitation (dark blue) data represent daytime mean values. Note that the shaded areas represent the model uncertainties.

development of the grass layer during this period (Figure 9). A fundamental aspect to remark here is that the E_s term should not be considered as solely soil evaporation but also direct evaporation from intercepted water by rain and/or dewfall, particularly during the wet period.

5. Discussion

A novel framework for the partitioning of net EC water fluxes into their constitutive terms *T* and E_s was developed and independently tested. The description of short-term χ variations, based on leaf-level optimality arguments up-scaled to canopy, was key to derive the optimal stomatal behavior in accordance with the inferred P_h patterns from EC. The combination of theory and observations provided the foundation for a data-model flux partitioning strategy that can be applied to the same spatiotemporal scales sampled by the EC footprint. The notion that stomata operate optimally to minimize water loss has been largely considered as the basis of the coupled plant carbon-water economies (Katul et al., 2000, 2010). It was even suggested to reflect a general evolutionary property attributed to all plant forms (Prentice et al., 2014). The timescales on which this theory is applicable is an important matter of debate (Buckley et al., 2017; Dewar et al., 2018). However, χ is expected to vary over the course of a day in response to diurnal *D* variations consistent with numerous leaf-gas exchange data and models, including optimality theories. The β parameter defining the "the carbon cost of water" was numerically solved over a 5-day window under the premise that a minimum water cost should hold while realistic diurnal g_c patterns were modeled based on well-defined environmental dependencies (i.e., *Q*, *D*, and T_{emp}). It is important to note that the optimal approximation for g_c was obtained without the need to disregard the influence of the canopy boundary layer. At the seasonal scale, χ variations were associated with soil moisture (Figure 3). This suggests that soil water availability is necessary in dynamic ecosystem models to constrain the temporal and spatial variability of χ and ultimately stomatal regulation and transpiration fluxes.

The proposed optimization scheme successfully interpreted the trade-off between χ and g_c according to the increased carbon cost of maintaining a given transpiration rate during drought conditions (Manzoni et al., 2013). Our findings showed that χ responded to soil dryness, when a reduction in g_c brought about a

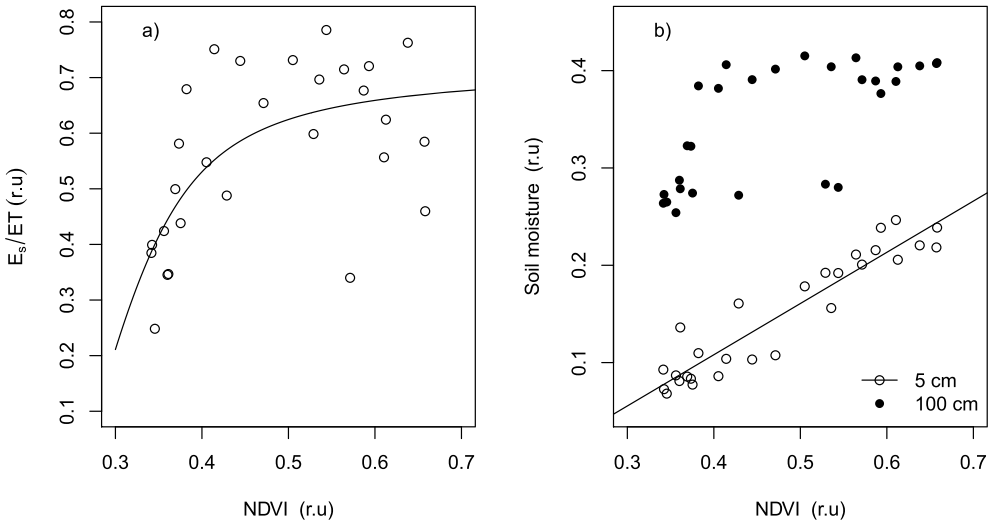

Figure 8. The relation between satellite-based normalized difference vegetation index (NDVI) and (a) E_s/ET and (b) soil moisture (SM) at 5- and 100-cm depth.

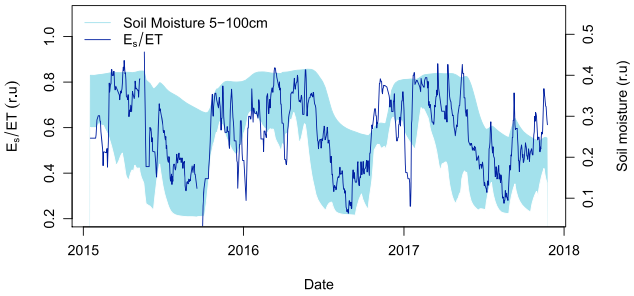

Figure 9. Seasonal variation of E_s/ET (%, dark blue) and soil moisture (%vol., light blue). The upper bound of the polygon represents the soil moisture at 100-cm depth, while the lowest bound the moisture at the shallow 5-cm depth.

decrease in χ during the summer drought (Figure S4) and subsequently an increased WUE (Figure S5). Though reducing the water cost is regarded here as the main benefit of an optimal stomata behavior, this pattern might reflect other associated costs (Wright et al., 2003). For instance, a complementary relationship between WUE and nitrogen-use efficiency has been well described through an optimization model by Palmroth et al. (2013). The fact that a higher WUE during water stress causes an increased foliar nitrogen (N) demand agrees with observations of N content in leaves in the Holm Oak (R. Cascon, personal communication, November 2017) and in the herbaceous layer (Migliavacca et al., 2017; Perez-Priego, Guan, et al., 2015). A higher allocation of N in photosynthetic proteins (i.e., increase in maximum carboxylation capacity, V_{cmax}) would eventually reduce the high cost of transpiration during the dry period. This also agrees with Wright et al. (2003), who suggested that the optimality theory is incomplete when the unit cost associated with photosynthesis is not considered. Presumably, a higher N investment in active photosynthetic proteins during the summer drought would support the evidence that a higher V_{cmax} per unit of leaf N area is found with increasing aridity (Prentice et al., 2011, 2014). Studies detailing changes in plant hydraulic properties associated with nitrogen availability and its interplay with WUE are required and make exciting future inquiry. As shown in Figures 5 and 6, improved partitioning FVS results can be achieved by accounting for mid-term and short-term biochemical kinetics of χ, which along with D define the observed seasonal variability of WUE.

The evaluation against independent data and methodology provides confidence that the proposed framework provides a practical approach for partitioning ET into its components from EC data (Figure S6). The proposed approach facilitates a broader exploration of how to approximate E_s/ET based on leaf area while accommodating the hydraulic properties of the soil. The dynamic of changes in E_s estimates agreed also with the empirical observations by Gardner (1959), who described the daily E_s decrease over the drying-down phase as a function of the square root of inverse time (r^2 = 0.99; Figure 10b). It is shown that the partitioning method provides a means for the retrieval not only of plant hydraulic properties but also for soil parameterization and model testing. For instance, Figure 10a illustrates the results of the alternative solution proposed by Brutsaert (2014), who proposed an exponential decay function of the form $E_s = E_0 \exp(-t/k)$ to parameterize soil physical characteristics. Note that E_0 represents the reference E_s at time 0 (t = 0) and k the decay (the higher the k, the slower is the decay of E_s). The optimized parameters E_0 and k of

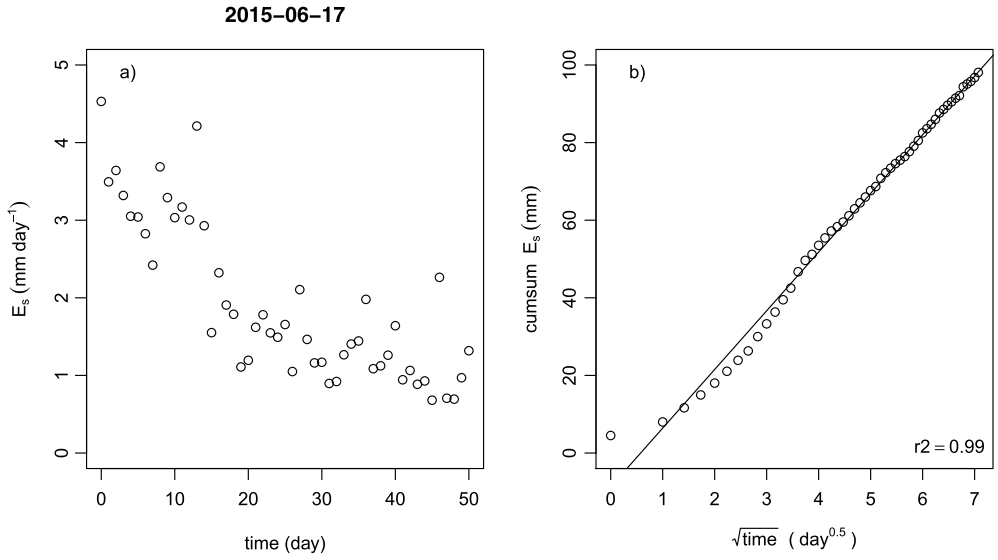

Figure 10. Daily patterns of (a) mean and (b) cumulative daily modeled E_s throughout the drying-down period presented in Figure 4. Data include 50 days starting from 17 June 2015. While an exponential decay function as proposed by Brutsaert (2014) was fitted to daily E_s (a), the widely used square root of inverse time was fitted to the cumulative E_s (b).

the empirical model were within the range of values reported for sandy-loam soil (Brutsaert, 2014) and along with FVS grant confidence to the partitioning method. By inferring WUE from optimality arguments, we have demonstrated the effectiveness of this approach when supplementing the FVS method, which is subjected to a number of differing assumptions and requirements including WUE parameterization. Comparison of FVS showed that the partitioned fluxes can be biased by up to 30% in average depending upon the WUE parameterization applied.

Our findings revealed that regardless of vegetation cover, E_s was larger than might be expected during both the growing-wet and dry conditions. While adequate soil moisture conditions allow high evaporative rates, E_s was largely sensitive to changes in climatic conditions (i.e., available energy and degree of aerodynamic coupling). This explains why E_s exhibited a highly dynamic behavior over the growing-to-dry transition period when the occurrence of precipitation was typically stochastic and the environmental conditions variable. During this period, rapid changes in E_s can be explained by a low soil hydraulic resistance of the top sandy layer, which favors evaporation in response to environmental changes (Figure 9). The large contribution of E_s to the total ET (approx. 70%) during the wet period agrees with Perez-Priego et al. (2017), who observed with lysimeters substantial moisture in the near-ground and plant surfaces that support the large contribution of the understory ET at our site. This pattern also agrees with Dubbert et al. (2014), who found with isotopes a significant contribution of E_s during the spring periods in a similar Mediterranean Savanna. This large contribution of E_s tends to agree with a compilation of global climate model-based estimates (Schlesinger & Jasechko, 2014). Perez-Priego et al. (2017) highlighted the nonnegligible role of nighttime dewfall, which should be regarded as an important source of E_s during the wet season. Conversely, a more sustained dynamic of E_s over the dry season is caused by the high hydraulic resistance of the clay layer in the deeper part of the soil. This decline was more accentuated than T, suggesting that the rooting system of the trees tap water from the deeper wet soil, which allowed them to sustain a relatively higher evaporation rates. As observed by lysimeter measurements, considerable E_s rates were measured when the shallow soil dried, indicating that the soil evaporative front should have held below the sandy layer.

6. Conclusions

Based on optimality arguments, we provide evidences that the dependency of χ on D is largely modulated by seasonal drought processes. Consequently, optimal stomatal models that assume β (or λ) as a functional attribute of plant forms might require adaptation to explicitly account for the temporal variability. This raises concerns when vegetation models use water stress factors to capture the seasonal variability but still assume β to be constant. Variations in β were shown not to alter the optimality predictions of g_c and χ when β is retained as part of the parameter optimization problem. The premise is that an optimal solution can be found for an objective function that minimizes the carbon cost of transpiration. We have demonstrated that adjustment in β along dry conditions can be numerically solved and provide a parsimonious representation of optimal stomatal behavior. When combined with EC data, this representation can elucidate plant and soil hydraulic properties. A realistic representation of individual E_s and T components is offered and shown to apply to the same spatiotemporal scales commensurate with EC-measured ET fluxes. The method developed here provides a practical and physiologically based water-flux partitioning framework and can be of general use across contrasting flux sites, biomes, and plant functional types. Clearly, the approach is most suitable to complement long-term flux measurements such as FLUXNET. Another pragmatic benefit of this approach is the indirect detection of mechanisms leading plants to functionally adapt and behave differently under contrasting conditions. Further research is needed to investigate the trade-off between water and nutrient in photosynthesis (e.g., using ecosystem-scale manipulative experiments; e.g., El-Madany et al., 2018), which is a topic best kept for the near future.

The approach proposed here could be most effective when supplementing other approaches such as FVS. Agreement among methods with differing assumptions and requirements lends confidence to the ET partitioning, and differences among methods can *flag* cases where further inquiry is required. Finally, the nonnegligible role of E_s over the whole range of conditions indicates that ET measurements by EC should be used with caution if they are assumed to be equivalent to T, particularly in (semi) arid sites. Soil moisture was the main driving factor of the seasonality of E_s/ET. In addition to soil moisture, other sources of E_s such as free evaporation of dew should not be overlooked.

Author Contributions

O. P. P. conceived and developed the method, performed the analysis, and wrote the manuscript. G. K. contributed to model development and provided written input. O. P. P., M. M., and M. R. designed the experimental setup; O. P. P., G. K., M. R., and M. M. contributed to the interpretation of the model. O. P. P. and B. A. developed the code. T. M. S. developed the FVS code. T. S. E. M. and A. C. processed the EC data. All authors contributed to the discussion and editing the paper.

Acknowledgments
The authors acknowledge the Alexander von Humboldt Foundation for supporting this research with the Max-Planck Prize to M. R. We acknowledge the city council of Majadas de Tiétar for its support. We thank Ulrich Weber and Xuanlong Ma for providing satellite NDVI data. The authors acknowledge Olaf Kolle and Martin Hertel from MPI-Jena, Gerardo M. Moreno from the University of Plasencia, and Ramon Lopez-Jimenez (CEAM) for technical assistance. EC data are available via the online repository (https://zenodo.org/record/1314194#.W09H-3qPWi5), while lysimeter data are available upon author request. The ET partitioning code is implemented in R (R Development Core Team, 2010) and freely available via the link https://github.com/oscarperezpriego/ETpartitioning. The FVS partitioning code can be used in an open source Python module under the link https://github.com/usda-ars-ussl/fluxpart (Skaggs et al., 2018).

References

Anderson, R. G., Zhang, X., & Skaggs, T. H. (2017). Measurement and partitioning of evapotranspiration for application to vadose zone studies. *Vadose Zone Journal*, *16*(13), 0. https://doi.org/10.2136/vzj2017.08.0155

Baldocchi, D., Falge, E., Gu, L., Olson, R., Hollinger, D., Running, S., et al. (2001). FLUXNET: A new tool to study the temporal and spatial variability of ecosystem-scale carbon dioxide, water vapor, and energy flux densities. *Bulletin of the American Meteorological Society*, *82*(11), 2415–2434. https://doi.org/10.1175/1520-0477(2001)082<2415:Fantts>2.3.Co;2

Ball, J. T., Woodrow, I. E., & Berry, J. A. (1987). A model predicting stomatal conductance and its contribution to the control of photosynthesis under different environmental conditions. In J. Biggins (Ed.), *Progress in photosynthesis research*, *Proceedings of the 7th International Congress on Photosynthesis* (Vol. 4, pp. 221–224). Dordrecht, The Netherlands: Martins Nijhoff.

Ball, T., & Berry, J. (1982). C_i/C_s ratio: A basis for predicting stomatal control of photosynthesis. *Carnegie Institution of Washington Year book*, *81*, 88–92.

Beer, C., Ciais, P., Reichstein, M., Baldocchi, D., Law, B. E., Papale, D., et al. (2009). Temporal and among-site variability of inherent water use efficiency at the ecosystem level. *Global Biogeochemical Cycles*, *23*, GB2018. https://doi.org/10.1029/2008GB003233

Berkelhammer, M., Noone, D. C., Wong, T. E., Burns, S. P., Knowles, J. F., Kaushik, A., et al. (2016). Convergent approaches to determine an ecosystem's transpiration fraction. *Global Biogeochemical Cycles*, *30*, 933–951. https://doi.org/10.1002/2016GB005392

Brutsaert, W. (2014). Daily evaporation from drying soil: Universal parameterization with similarity. *Water Resources Research*, *50*, 3206–3215. https://doi.org/10.1002/2013WR014872

Buckley, T. N. (2017). Modeling stomatal conductance. *Plant Physiology*, *174*(2), 572–582. https://doi.org/10.1104/pp.16.01772

Buckley, T. N., Sack, L., & Farquhar, G. D. (2017). Optimal plant water economy. *Plant, Cell & Environment*, *40*(6), 881–896. https://doi.org/10.1111/pce.12823

Cowan, I., & Farquhar, G. (1977). Stomatal function in relation to leaf metabolism and environment, paper presented at Symposia of the Society for Experimental Biology.

de Dios, V. R., Roy, J., Ferrio, J. P., Alday, J. G., Landais, D., Milcu, A., & Gessler, A. (2015). Processes driving nocturnal transpiration and implications for estimating land evapotranspiration. *Scientific Reports*, *5*(1), 10975. https://doi.org/10.1038/srep10975

Development Core Team, R. (2010). *R: A language and environment for statistical computing*. Vienna, Austria: R Foundation for Statistical Computing. Retrieved from http://www.R-project.org

Dewar, R., Mauranen, A., Makela, A., Holtta, T., Medlyn, B., & Vesala, T. (2018). New insights into the covariation of stomatal, mesophyll and hydraulic conductances from optimization models incorporating nonstomatal limitations to photosynthesis. *The New Phytologist*, *217*(2), 571–585. https://doi.org/10.1111/nph.14848

Dubbert, M., Piayda, A., Cuntz, M., Correia, A. C., Costa, E. S. F., Pereira, J. S., & Werner, C. (2014). Stable oxygen isotope and flux partitioning demonstrates understory of an oak savanna contributes up to half of ecosystem carbon and water exchange. *Frontiers in Plant Science*, *5*, 530. https://doi.org/10.3389/fpls.2014.00530

El-Madany, T. R., Reichstein, M., Perez-Priego, O., Carrara, A., Moreno, G., Martín, M. P., et al. (2018). Drivers of spatio-temporal variability of carbon dioxide and energy 1 fluxes in a Mediterranean savanna ecosystem. *Agricultural and Forest Meteorology*, *262*, 258–278. https://doi.org/10.1016/j.agrformet.2018.07.010

Finkelstein, P. L., & Sims, P. F. (2001). Sampling error in eddy correlation flux measurements. *Journal of Geophysical Research*, *106*(D4), 3503–3509. https://doi.org/10.1029/2000JD900731

Fisher, J. B., Melton, F., Middleton, E., Hain, C., Anderson, M., Allen, R., et al. (2017). The future of evapotranspiration: Global requirements for ecosystem functioning, carbon and climate feedbacks, agricultural management, and water resources. *Water Resources Research*, *53*, 2618–2626. https://doi.org/10.1002/2016WR020175

Fites, J. A., & Teskey, R. O. (1988). CO_2 and water vapor exchange of Pinustaeda in relation to stomatal behavior: Test of an optimization hypothesis. *Canadian Journal of Forest Research*, *18*(2), 150–157. https://doi.org/10.1139/x88-024

Fratini, G., & Mauder, M. (2014). Towards a consistent eddy-covariance processing: An intercomparison of EddyPro and TK3. *Atmospheric Measurement Techniques*, *7*(7), 2273–2281. https://doi.org/10.5194/amt-7-2273-2014

Gardner, W. R. (1959). Solutions of the flow equation for the drying of soils and other porous media. *Soil Science Society of America Journal*, *23*(3), 183–187. https://doi.org/10.2136/sssaj1959.03615995002300030010x

Gelman, A., & Shirley, K. (2011). Inference from simulations and monitoring convergence. In *Handbook of Markov chain Monte Carlo* (pp. 163–174). New York: Chapman and Hall/CRC.

Hari, P., Makela, A., & Pohja, T. (2000). Surprising implications of the optimality hypothesis of stomatal regulation gain support in a field test. *Australian Journal of Plant Physiology*, *27*(1), 77–80. https://doi.org/10.1071/PP99050

Hetherington, A. M., & Woodward, F. I. (2003). The role of stomata in sensing and driving environmental change. *Nature*, *424*(6951), 901–908. https://doi.org/10.1038/nature01843

Hicks, B. B., Baldocchi, D. D., Meyers, T. P., Hosker, R. P., & Matt, D. R. (1987). A preliminary multiple resistance routine for deriving dry deposition velocities from measured quantities. *Water, Air, and Soil Pollution*, *36*(3–4), 311–330. https://doi.org/10.1007/Bf00229675

IUSS Working Group WRB (2015). World reference base for soil resources 2014, update 2015. International soil classification system for naming soils and creating legends for soil maps. World Soil Resources Reports No. 106. FAO, Rome.

James, I. L. M., & Gifford, R. M. (1983). Stomatal sensitivity to carbon dioxide and humidity: A comparison of two C_3 and two C_4 grass species. *Plant Physiology*, *71*(4), 789–796.

Jarvis, P. G. (1976). The interpretation of the variations in leaf water potential and stomatal conductance found in canopies in the field. *Philosophical Transactions of the Royal Society of London*, *273B*, 593–610.

Jarvis, P. G., & McNaughton, K. G. (1986). Stomatal control of transpiration: Scaling up from leaf to region. *Advances in Ecological Research*, *15*, 1–49. https://doi.org/10.1016/S0065-2504(08)60119-1

Jones, H. G. (1998). Stomatal control of photosynthesis and transpiration. *Journal of Experimental Botany*, *49*(90001), 387–398. https://doi.org/10.1093/jexbot/49.suppl_1.387

Katul, G., Ellsworth, D. S., & Lai, C. T. (2000). Modelling assimilation and intercellular CO_2 from measured conductance: A synthesis of approaches. *Plant, Cell and Environment*, *23*(12), 1313–1328. https://doi.org/10.1046/j.1365-3040.2000.00641.x

Katul, G., Leuning, R., & Oren, R. (2003). Relationship between plant hydraulic and biochemical properties derived from a steady-state coupled water and carbon transport model. *Plant, Cell and Environment*, *26*(3), 339–350. https://doi.org/10.1046/j.1365-3040.2003.00965.x

Katul, G., Manzoni, S., Palmroth, S., & Oren, R. (2010). A stomatal optimization theory to describe the effects of atmospheric CO_2 on leaf photosynthesis and transpiration. *Annals of Botany*, *105*(3), 431–442. https://doi.org/10.1093/aob/mcp292

Katul, G., Oren, R., Manzoni, S., Higgins, C., & Parlange, M. B. (2012). Evapotranspiration: A process driving mass transport and energy exchange in the soil-plant-atmosphere-climate system. *Reviews of Geophysics*, *50*, RG3002. https://doi.org/10.1029/2011RG000366

Katul, G. G., Palmroth, S., & Oren, R. (2009). Leaf stomatal responses to vapour pressure deficit under current and CO_2-enriched atmosphere explained by the economics of gas exchange. *Plant, Cell & Environment*, *32*(8), 968–979. https://doi.org/10.1111/j.1365-3040.2009.01977.x

Lasslop, G., Reichstein, M., Papale, D., Richardson, A. D., Arneth, A., Barr, A., et al. (2010). Separation of net ecosystem exchange into assimilation and respiration using a light response curve approach: Critical issues and global evaluation. *Global Change Biology*, *16*(1), 187–208. https://doi.org/10.1111/j.1365-2486.2009.02041.x

Leuning, R. (1990). Modelling stomatal behaviour and and photosynthesis of Eucalyptus grandis. *Australian Journal of Plant Physiology*, *17*(2), 159–175. https://doi.org/10.1071/PP9900159

Leuning, R. (1995). A critical appraisal of a combined stomatal-photosynthesis model for C_3 plants. *Plant, Cell and Environment*, *18*(4), 339–355. https://doi.org/10.1111/j.1365-3040.1995.tb00370.x

Lin, Y. S., Medlyn, B. E., Duursma, R. A., Prentice, I. C., Wang, H., Baig, S., et al. (2015). Optimal stomatal behaviour around the world. *Nature Climate Change*, *5*(5), 459–464. https://doi.org/10.1038/Nclimate2550

Manzoni, S., Vico, G., Palmroth, S., Porporato, A., & Katul, G. (2013). Optimization of stomatal conductance for maximum carbon gain under dynamic soil moisture. *Advances in Water Resources*, *62*, 90–105. https://doi.org/10.1016/j.advwatres.2013.09.020

Mauder, M., & Foken, T. (2004). *Documentation and instruction manual of the eddy covariance software package TK2* (45 pp.). Universität Bayreuth, Bayreuth.

Medlyn, B. E., Duursma, R. A., Eamus, D., Ellsworth, D. S., Prentice, I. C., Barton, C. V. M., et al. (2011). Reconciling the optimal and empirical approaches to modelling stomatal conductance. *Global Change Biology*, *17*(6), 2134–2144. https://doi.org/10.1111/j.1365-2486.2010.02375.x

Migliavacca, M., Meroni, M., Manca, G., Matteucci, G., Montagnani, L., Grassi, G., et al. (2009). Seasonal and interannual patterns of carbon and water fluxes of a poplar plantation under peculiar eco-climatic conditions. *Agricultural and Forest Meteorology*, *149*(9), 1460–1476. https://doi.org/10.1016/j.agrformet.2009.04.003

Migliavacca, M., Perez-Priego, O., Rossini, M., el-Madany, T. S., Moreno, G., van der Tol, C., et al. (2017). Plant functional traits and canopy structure control the relationship between photosynthetic CO_2 uptake and far-red sun-induced fluorescence in a Mediterranean grassland under different nutrient availability. *The New Phytologist*, *214*(3), 1078–1091. https://doi.org/10.1111/nph.14437

Monteith, J. L., & Unsworth, M. H. (2013). Chapter 17—Micrometeorology: (ii) Interpretation of flux measurements. In *Principles of environmental physics* (4th ed., pp. 321–349). Boston: Academic Press. https://doi.org/10.1016/B978-0-12-386910-4.00017-2

Mortazavi, B., Chanton, J. P., Prater, J. L., Oishi, A. C., Oren, R., & Katul, G. (2005). Temporal variability in ^{13}C of respired CO_2 in a pine and a hardwood forest subject to similar climatic conditions. *Oecologia*, *142*(1), 57–69. https://doi.org/10.1007/s00442-004-1692-2

Norman, J. M. (1982). Simulation of microclimates. In J. L. Hatfield & I. J. Thomason (Eds.), *Biometeorology in integrated pest management* (pp. 65–99). Cambridge, MA: Academic Press. https://doi.org/10.1016/B978-0-12-332850-2.50009-8

Novick, K. A., Oren, R., Stoy, P. C., Siqueira, M. B. S., & Katul, G. G. (2009). Nocturnal evapotranspiration in eddy-covariance records from three co-located ecosystems in the southeastern U.S.: Implications for annual fluxes. *Agricultural and Forest Meteorology*, *149*(9), 1491–1504. https://doi.org/10.1016/j.agrformet.2009.04.005

Palatella, L., Rana, G., & Vitale, D. (2014). Towards a flux-partitioning procedure based on the direct use of high-frequency eddy-covariance data. *Boundary-Layer Meteorology*, *153*(2), 327–337. https://doi.org/10.1007/s10546-014-9947-x

Palmroth, S., Katul, G. G., Maier, C. A., Ward, E., Manzoni, S., & Vico, G. (2013). On the complementary relationship between marginal nitrogen and water-use efficiencies among *Pinus taeda* leaves grown under ambient and CO_2-enriched environments. *Annals of Botany*, *111*(3), 467–477. https://doi.org/10.1093/aob/mcs268

Perez-Priego, O., el-Madany, T. S., Migliavacca, M., Kowalski, A. S., Jung, M., Carrara, A., et al. (2017). Evaluation of eddy covariance latent heat fluxes with independent lysimeter and sapflow estimates in a Mediterranean savannah ecosystem. *Agricultural and Forest Meteorology*, *236*, 87–99. https://doi.org/10.1016/j.agrformet.2017.01.009

Perez-Priego, O., Guan, J., Rossini, M., Fava, F., Wutzler, T., Moreno, G., et al. (2015). Sun-induced chlorophyll fluorescence and photochemical reflectance index improve remote-sensing gross primary production estimates under varying nutrient availability in a typical Mediterranean savanna ecosystem. *Biogeosciences*, *12*(21), 6351–6367. https://doi.org/10.5194/bg-12-6351-2015

Perez-Priego, O., Lopez-Ballesteros, A., Sanchez-Canete, E. P., Serrano-Ortiz, P., Kutzbach, L., Domingo, F., et al. (2015). Analysing uncertainties in the calculation of fluxes using whole-plant chambers: Random and systematic errors. *Plant and Soil*, *393*(1–2), 229–244. https://doi.org/10.1007/s11104-015-2481-x

Prentice, I. C., Dong, N., Gleason, S. M., Maire, V., & Wright, I. J. (2014). Balancing the costs of carbon gain and water transport: Testing a new theoretical framework for plant functional ecology. *Ecology Letters*, *17*(1), 82–91. https://doi.org/10.1111/ele.12211

Prentice, I. C., Meng, T., Wang, H., Harrison, S. P., Ni, J., & Wang, G. (2011). Evidence of a universal scaling relationship for leaf CO_2 drawdown along an aridity gradient. *The New Phytologist*, *190*(1), 169–180. https://doi.org/10.1111/j.1469-8137.2010.03579.x

Reichstein, M., Falge, E., Baldocchi, D., Papale, D., Aubinet, M., Berbigier, P., et al. (2005). On the separation of net ecosystem exchange into assimilation and ecosystem respiration: Review and improved algorithm. *Global Change Biology*, *11*(9), 1424–1439. https://doi.org/10.1111/j.1365-2486.2005.001002.x

Reichstein, M., Tenhunen, J., Roupsard, O., Ourcival, J. M., Rambal, S., Miglietta, F., et al. (2003). Inverse modeling of seasonal drought effects on canopy CO_2/H_2O exchange in three Mediterranean ecosystems. *Journal of Geophysical Research*, *108*(D23), 4726. https://doi.org/10.1029/2003JD003430

Reth, S., Seyfarth, M., Gefke, O., & Friedrich, H. (2007). Lysimeter soil retriever (LSR)—A new technique for retrieving soil from lysimeters for analysis. *Journal of Plant Nutrition and Soil Science*, *170*(3), 345–346. https://doi.org/10.1002/jpln.200625069

Scanlon, T. M., & Kustas, W. P. (2010). Partitioning carbon dioxide and water vapor fluxes using correlation analysis. *Agricultural and Forest Meteorology*, *150*(1), 89–99. https://doi.org/10.1016/j.agrformet.2009.09.005

Scanlon, T. M., & Kustas, W. P. (2012). Partitioning evapotranspiration using an eddy covariance-based technique: Improved assessment of soil moisture and land-atmosphere exchange dynamics. *Vadose Zone Journal*, *11*(3). https://doi.org/10.2136/vzj2012.0025

Scanlon, T. M., & Sahu, P. (2008). On the correlation structure of water vapor and carbon dioxide in the atmospheric surface layer: A basis for flux partitioning. *Water Resources Research*, *44*, W10418. https://doi.org/10.1029/2008WR006932

Schlesinger, W. H., & Jasechko, S. (2014). Transpiration in the global water cycle. *Agricultural and Forest Meteorology*, *189-190*, 115–117. https://doi.org/10.1016/j.agrformet.2014.01.011

Scott, R. L., & Biederman, J. A. (2017). Partitioning evapotranspiration using long-term carbon dioxide and water vapor fluxes. *Geophysical Research Letters*, *44*, 6833–6840. https://doi.org/10.1002/2017GL074324

Skaggs, T. H., Anderson, R. G., Alfieri, J. G., Scanlon, T. M., & Kustas, W. P. (2018). Fluxpart: Open source software for partitioning carbon dioxide and water vapor fluxes. *Agricultural and Forest Meteorology*, *253-254*, 218–224. https://doi.org/10.1016/j.agrformet.2018.02.019

Sulman, B. N., Roman, D. T., Scanlon, T. M., Wang, L., & Novick, K. A. (2016). Comparing methods for partitioning a decade of carbon dioxide and water vapor fluxes in a temperate forest. *Agricultural and Forest Meteorology*, *226-227*, 229–245. https://doi.org/10.1016/j.agrformet.2016.06.002

Tan, Z. H., Wu, Z. X., Hughes, A. C., Schaefer, D., Zeng, J., Lan, G. Y., et al. (2017). On the ratio of intercellular to ambient CO_2 (c_i/c_a) derived from ecosystem flux. *International Journal of Biometeorology*, *61*(12), 2059–2071. https://doi.org/10.1007/s00484-017-1403-4

Twine, T. E., Kustas, W. P., Norman, J. M., Cook, D. R., Houser, P. R., Meyers, T. P., et al. (2000). Correcting eddy-covariance flux underestimates over a grassland. *Agricultural and Forest Meteorology*, *103*(3), 279–300. https://doi.org/10.1016/S0168-1923(00)00123-4

Villalobos, F. J., Perez-Priego, O., Testi, L., Morales, A., & Orgaz, F. (2012). Effects of water supply on carbon and water exchange of olive trees. *European Journal of Agronomy*, *40*, 1–7. https://doi.org/10.1016/j.eja.2012.02.004

Volpe, V., Manzoni, S., Marani, M., & Katul, G. (2011). Leaf conductance and carbon gain under salt-stressed conditions. *Journal of Geophysical Research*, *116*, G04035. https://doi.org/10.1029/2011JG001848

Wang, H., Prentice, I. C., & Davis, T. W. (2014). Biophysical constraints on gross primary production by the terrestrial biosphere. *Biogeosciences*, *11*(20), 5987–6001. https://doi.org/10.5194/bg-11-5987-2014

Wang, H., Prentice, I. C., Keenan, T. F., Davis, T. W., Wright, I. J., Cornwell, W. K., et al. (2017). Towards a universal model for carbon dioxide uptake by plants. *Nature Plants*, *3*(9), 734–741. https://doi.org/10.1038/s41477-017-0006-8

Wang, W., Smith, J. A., Ramamurthy, P., Baeck, M. L., Bou-Zeid, E., & Scanlon, T. M. (2016). On the correlation of water vapor and CO_2: Application to flux partitioning of evapotranspiration. *Water Resources Research*, *52*, 9452–9469. https://doi.org/10.1002/2015WR018161

Way, D. A., Oren, R., Kim, H.-S., & Katul, G. G. (2011). How well do stomatal conductance models perform on closing plant carbon budgets? A test using seedlings grown under current and elevated air temperatures. *Journal of Geophysical Research*, *116*, G04031. https://doi.org/10.1029/2011JG001808

Wehr, R., Commane, R., Munger, J. W., McManus, J. B., Nelson, D. D., Zahniser, M. S., et al. (2017). Dynamics of canopy stomatal conductance, transpiration, and evaporation in a temperate deciduous forest, validated by carbonyl sulfide uptake. *Biogeosciences*, *14*(2), 389–401. https://doi.org/10.5194/bg-14-389-2017

Wei, Z. W., Yoshimura, K., Wang, L. X., Miralles, D. G., Jasechko, S., & Lee, X. H. (2017). Revisiting the contribution of transpiration to global terrestrial evapotranspiration. *Geophysical Research Letters*, *44*, 2792–2801. https://doi.org/10.1002/2016GL072235

Wong, S. C., Cowan, I. R., & Farquhar, G. D. (1979). Stomatal conductance correlates with photosynthetic capacity. *Nature*, *282*(5737), 424–426. https://doi.org/10.1038/282424a0

Wright, I. J., Reich, P. B., & Westoby, M. (2003). Least-cost input mixtures of water and nitrogen for photosynthesis. *The American Naturalist*, *161*(1), 98–111. https://doi.org/10.1086/344920

Wutzler, T., Lucas-Moffat, A., Migliavacca, M., Knauer, J., Sickel, K., Šigut, L., et al. (2018). Basic and extensible post-processing of eddy covariance flux data with REddyProc. *Biogeosciences Discussions*, *2018*, 1–39. https://doi.org/10.5194/bg-2018-56

Zhou, S., Yu, B., Zhang, Y., Huang, Y., & Wang, G. (2016). Partitioning evapotranspiration based on the concept of underlying water use efficiency. *Water Resources Research*, *52*, 1160–1175. https://doi.org/10.1002/2015WR017766